

## A RECONFIGURABLE GUIDANCE APPROACH FOR REUSABLE LAUNCH VEHICLES

J. D. Schierman\* D.G. Ward† J.F. Monaco‡ J.R. Hull§  
Barron Associates, Inc., Charlottesville, Virginia

### Abstract

A guidance system with reconfiguration capabilities has been developed for reusable launch vehicles (RLVs). The focus of the development is on reconfiguration after a catastrophic effector failure during final approach – a failure that would otherwise cause loss of the vehicle. We assume here that the vehicle employs a reconfigurable inner-loop control system that recovers some maneuvering capabilities and maintains attitude stability. However, for RLVs, it is often the case that nominal performance cannot be fully recovered, and the outer-loop guidance system must account for the degraded response characteristics. Two approaches are presented. The first approach augments the existing production guidance system with adaptation capabilities. A case study shows that stability is maintained following a primary pitch effector failure. However, it is shown that the trajectory commands to the guidance loops must also be re-targeted in order to achieve a safe landing. The second approach employs an on-line optimal trajectory re-targeting algorithm. A database of neighboring optimal trajectories is encoded in an efficient manner and interrogated on line at regular intervals. Given the current states and certain vehicle parameters, this procedure generates optimal guidance commands and integrates the optimal trajectory to the next update point. A proof-of-concept study of this approach was performed. Following a primary speed control failure, the study shows that this approach achieves acceptable landing conditions.

### Introduction

Increasing the reliability and safety of next generation launch vehicles is of primary concern for NASA, the Air Force and several other organizations involved in the advancement of space access technologies. [1] It is widely recognized that on-board reconfiguration capabilities will be *essential* to achieve these increased levels of reliability. For Hypersonic Reusable Launch Vehicles (RLVs), vehicle attitude and flight path must be tightly controlled throughout a very wide flight envelope to ensure that the airframe remains within a number of different constraints (thermal, structural, stability, etc). In some cases (e.g., re-entry or auto-landing), the "corridor" of allowable trajectories may be quite narrow. Further, there are unique challenges in determining the dynamics of these vehicles compared to other fixed-wing aircraft. Two key difficulties are that high-Mach wind tunnel tests are less representative of the actual aircraft dynamics, and at hypersonic velocities, accurate measurements can be difficult to obtain, making parameter identification from flight data more challenging than with conventional aircraft. Added to this uncertainty is the possibility that failure of a critical control component (e.g., elevon effector) might drive the vehicle to near or beyond its allowable guidance corridor limits. If the control and guidance systems are not quickly reconfigured, recovery of the vehicle might not be possible.

Furthermore, RLV designs are influenced by weight and other constraints that rarely allow for significant effector redundancy to *completely* recover the pre-failure closed-loop dynamics using inner-loop reconfiguration strategies alone. Therefore, it is likely that the closed-loop dynamics will change even after inner-loop reconfiguration. This leads to the desire to investigate adaptive autonomous control *and* guidance systems that reconfigure for unforeseen dynamics in the inner-loop to the extent possible and then *recompute* realizable guidance trajectories and autopilot commands based on the new inner-loop dynamics and possibly evolving mission objectives.

---

\* Research Scientist, Senior Member  
† Senior Research Scientist, Member  
‡ Senior Research Scientist, Member  
§ Research Associate

The focus of this paper is on the development of an adaptive guidance system that would ultimately work in conjunction with an inner-loop reconfigurable control system.

### Demonstration Platform

Orbital Science Corporation's X-34 hypersonic rocket plane, shown in Figure 1, was used as the demonstration platform in the developments presented herein [2-3]. It is a reusable, suborbital, air-launched vehicle designed to operate in a broad hypersonic flight envelope of speeds approaching Mach 8 at altitudes up to 50 miles. It was designed to be air-launched from Orbital's L-1011 Tri-Star carrier aircraft currently used to launch the Pegasus expendable launch vehicle. The vehicle weighs approximately 17,000 lb. and its power-plant is the Fastrac single-stage engine that burns a mixture of liquid oxygen and kerosene.



Figure 1. Orbital Sciences Corp. X-34 Hypersonic Reusable Launch Vehicle.

The program planned for production of three X-34 vehicles, with the final vehicle earmarked for a series of powered flight tests beginning in approximately the year 2002. One of the main objectives of the X-34 program was to develop and demonstrate advanced technologies to benefit future hypersonic RLV production systems. However, NASA recently made a major shift in its long-term directions for the development of the next generation RLV. Several of the X-plane development programs, including the X-33 and the X-34 were cancelled. Nonetheless, the technologies developed herein are broadly applicable to this class of vehicles, and we continue to mature the approaches for other X-plane programs.

The focus of the study presented here is on the longitudinal motion of the vehicle during the approach-to-landing phase of flight. The X-34's primary control effectors in this phase are elevons to control pitching motion, speedbrake to adjust velocity due to head/tail winds and reject gust disturbances, and body flap for pitch trim adjustment.

### The Overall Guidance Approach

Figure 2 presents the high level architecture of our guidance approach. There are two main aspects to this approach.

1. The outer-loop independently identifies inner-closed-loop dynamics and guidance reconfiguration acts *independent* of the inner-loop reconfiguration.
2. The guidance system incorporates a long-horizon on-line trajectory re-targeting algorithm that drives a primary adaptable guidance system. The primary guidance system is tasked to maintain flight stability - critical during the recovery stage from an effector failure. The primary guidance system is updated sufficiently fast enough to run in real time. In contrast, the trajectory re-targeting algorithm is expected to be computationally more intensive, and will run in *near* real-time, at a slower update rate.

The objective of this *modular* approach is to enable more freedom in the development/implementation of such a system. The designer can choose between several options for inner-loop control reconfiguration, primary guidance adaptation and trajectory re-targeting schemes to best fit the needs of the particular application.

The two main guidance system approaches are discussed next.

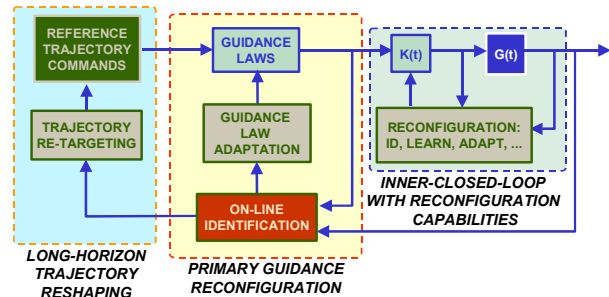


Figure 2. High Level Architecture for Reconfigurable Control/Guidance System.

## Adaptive Production Guidance (APG) Approach

This approach integrates reconfiguration capabilities into the current production guidance system. The APG approach should offer a lower-risk, nearer-term solution to maintain flight stability and improve performance under effector failures or significant aerodynamic modeling errors.

A simplified representation of the altitude guidance loops for this approach is given in Figure 3. Here, the primary guidance module includes a gain adaptation algorithm that varies the feedback gains on altitude and altitude rate errors, depending on the current estimate of inner-loop capabilities. The figure indicates that the Modified Sequential Least Squares (MSLS) parameter identification algorithm [4] provides information regarding the current capabilities of the inner-closed-loop system to the adaptation algorithm. It will be shown that this method provides rapid gain adaptation to maintain stability immediately following a severe elevon failure that significantly reduces the inner-loop bandwidth.

Figure 3 also shows reconfiguration of the reference command signals. Here, the parameter identification algorithm provides information to a reference altitude and altitude rate command adaptation algorithm. It is shown that reconfiguration of these reference command signals is necessary to safely land the vehicle. A simplified re-targeting scheme was investigated for the case study, discussed next.

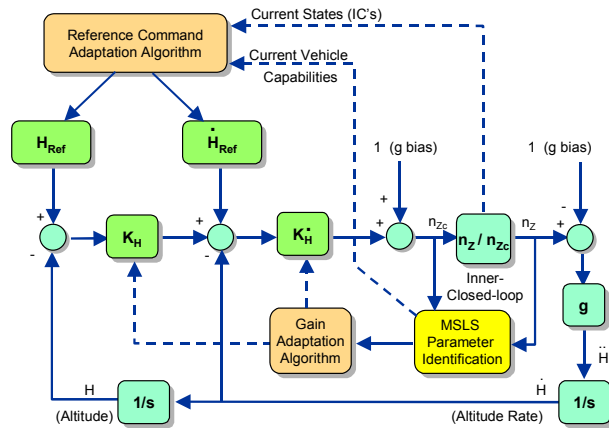


Figure 3. Altitude Guidance Loops for Adaptive Production Guidance (APG) System.

## Case Study: APG Approach

A preliminary study of the X-34 approach-to-landing problem with elevon failures is presented. Altitude, velocity, and flight path profiles specific to the X-34's approach-to-landing trajectory have been provided by Orbital and integrated into the study. Further, the altitude and altitude rate guidance loop architectures used in this study closely approximate the production guidance system used on the X-34 vehicle.

The inner-closed-loop vehicle is represented by the transfer function from normal acceleration to its respective command, or  $n_z/n_{zc}$ . Here,

$$\frac{n_z(s)}{n_{zc}(s)} = \left( \frac{-\omega_n^2}{z^2} \right) \frac{(s+z)(s-z)}{s^2 + 2\zeta\omega_n s + \omega_n^2} \quad (1)$$

where,

$$\begin{aligned} z &= 2 \text{ rad/sec (zero location)} \\ \zeta &= 0.6 \text{ (inner-closed-loop damping)} \end{aligned} \quad (2)$$

### Nominal System Results

For the nominal system, the inner-closed-loop natural frequency was:

$$\omega_n = 1.6 \text{ rad/sec} \quad (3)$$

The feedback gains were chosen to be:

$$K_H = 0.39 \ \& \ K_{\dot{H}} = 0.022 \quad (4)$$

These values can be shown to give at least 6 dB of gain margin and over 45 degrees of phase margin for each loop.

Figure 4 presents a close up of the nominal vehicle's approach-to-landing trajectory near landing, starting from an altitude of 10,000 ft. Trajectory integration actually began at an altitude of 30,000 ft. Note that the altitude plotted is altitude above the runway, not above sea level. Both the altitude reference command ( $H_{Ref}$ ) and the altitude response ( $H$ ) are plotted. It is evident that the vehicle follows the reference command quite accurately. The trajectory begins at a steep glideslope with a flight path angle = -17 deg. Here, it can be seen that after the first flare, the glideslope becomes quite shallow, and the flight path angle rapidly reduces from -2 degrees to near zero degrees at landing. Although not simulated, a final flare maneuver would be executed just before landing to make final adjustments to the terminal velocity and arrest the touchdown sink rate.

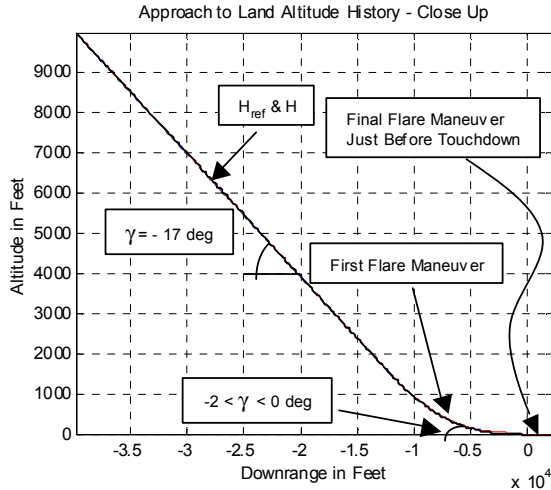


Figure 4. Nominal Vehicle's Approach-to-Landing Trajectory.

Figure 5 presents the sink rate time history for the nominal vehicle. Again, the vehicle's response closely follows the reference command signal. The sink rate approaches near zero at touchdown. The performance of the nominal design is considered to be excellent.

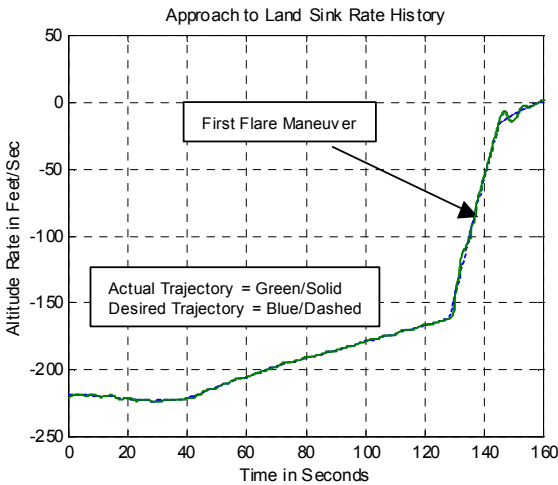


Figure 5. Nominal Vehicle's Sink Rate Time History.

#### Failed Elevon/No Guidance Reconfiguration Results

We now consider an elevon failure. We assume that an inner-loop control reconfiguration will properly adapt to a failed elevon by controlling pitch attitude dynamics with the only other available pitch control effectors, body flap and speed brake. However, nominal performance can never be recovered in this case because the bandwidths of the body flap and speed brake are much slower than that of the elevon effector. Under an elevon failure, inner-loop reconfiguration is

expected to reduce the natural frequency in the normal acceleration transfer function (see Eq. (1)) to approximately:

$$\omega_h = 0.4 \text{ rad/sec} \quad (5)$$

The elevon failure was modeled to occur at 80 seconds into the flight (approximately 10,000 ft in altitude) by appropriately reducing  $\omega_h$  to the value given in Eq. (5) at that time.

Figure 6 presents the approach-to-landing trajectory for this case *when no outer-loop guidance reconfiguration was mechanized*. The altitude and altitude rate loop gains were held constant at their nominal values. It can be seen in the figure that without guidance reconfiguration, the vehicle's trajectory goes unstable, resulting in loss of the vehicle.

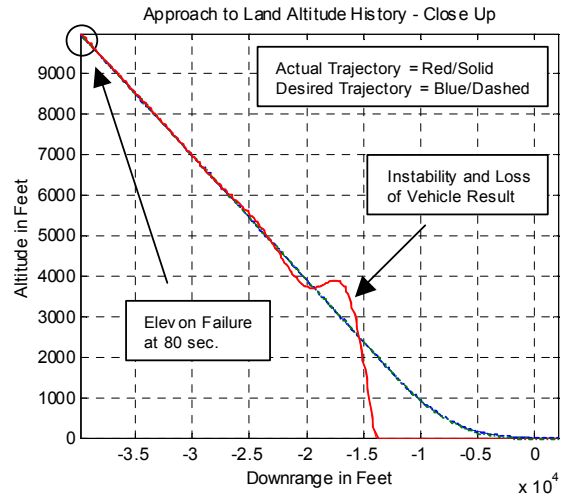


Figure 6. Approach-to-Land Trajectory Under Elevon Failure - With No Guidance Reconfiguration.

#### Failed Elevon With Guidance Reconfiguration

We next integrated a primary guidance reconfiguration scheme into the system. This included a Modified Sequential Least Squares (MSLS) algorithm [4] coupled with a guidance gain adaptation law (see Figure 3). In a sequential loop closure fashion, several loop gain values for the altitude and altitude rate loops were designed as the inner-loop bandwidth was ranged from its nominal value to the value under speed brake/body flap reconfiguration. The gain values were designed to achieve gain margins between 6 and 7 dB and phase margins not less than 45 degrees. For computational efficiency, the gain adaptation algorithm was defined as curve fits to the design data. The gain adaptation laws were:

$$\begin{aligned}
 K_H &= -1.3510e-001 \Omega + 7.1888e-002 \\
 K_{\dot{H}} &= -2.5736e-003 \Omega^3 - 1.2776e-002 \Omega^2 \\
 &\quad - 2.3127e-002 \Omega + 3.3534e-003 \quad (6)
 \end{aligned}$$

where  $\Omega = -\omega_n^2$ , and  $\omega_n$  is the inner-closed-loop bandwidth (see Eq. (1)). These functions were defined in this manner because the MSLS algorithm directly identifies the parameter  $\Omega$ .

Figure 7 plots the adaptation laws given by Eq. (6), and the corresponding design data. It was determined by simulation that the accuracies of the curve fits were adequate.

Next, we turn our attention to the MSLS identification results. To model the real world effects of measurement noise, subsequent filtering and state reconstruction, filtered noise was added to the outputs of the inner-closed-loop model. Figure 8 presents the inner-loop bandwidth parameter,  $\Omega$ , and its MSLS estimate. Note that identification of the new value at 80 seconds is almost immediate. The reason for such rapid identification is that at the time of failure there is a substantial change in the inner-closed-loop responses, which, due to feedback, excites the commanded acceleration into the inner-closed-loop system (not shown). Because of this rapid excitation, the new values for the model parameters are quickly identified. In reality, since the inner-loop control system may take time to reconfigure to the slower control effectors, identification of the new bandwidth may not be as rapid as shown here. However, as shown in Figure 6, the vehicle travels for approximately 17,000 ft (or, approximately, 25 seconds) before significantly departing from the nominal trajectory. Real world effects such as wind gusts will most likely cause the instability to appear sooner than this, but based on past experience, the benign flight characteristics of an RLV's entry/approach should allow for enough time for both the inner and outer-loop identification and reconfiguration procedures to stabilize the system.

Figure 9 presents the altitude and altitude rate loop gain time histories. Because of the rapid identification of the change in the inner-loop bandwidth, these gains also rapidly change to their new values corresponding to adaptation laws given in Eq. (6). Note that the time histories seen in both Figure 8 and Figure 9 are more irregular before the elevon failure and smoother afterwards. Again, this is due low excitation of the system preceding the failure and increased control activity following the failure.

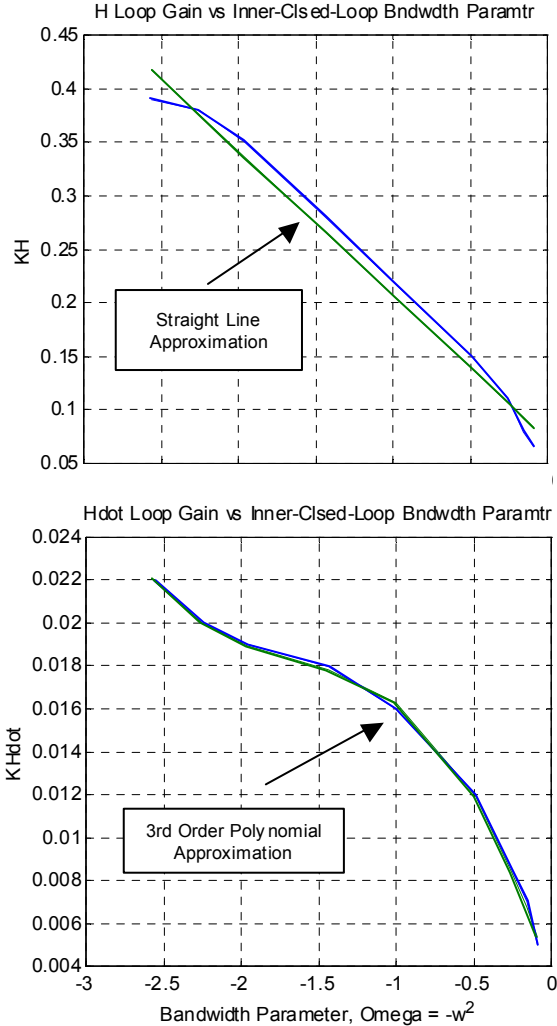


Figure 7. Loop Gains For Acceptable Margins.

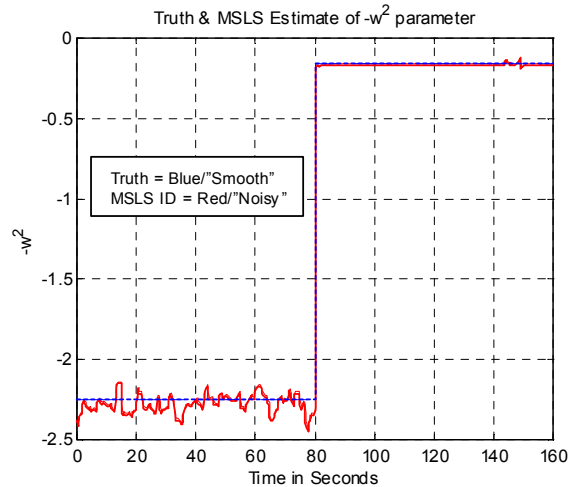


Figure 8. MSLS Estimate of Bandwidth Parameter,  $\Omega$ .

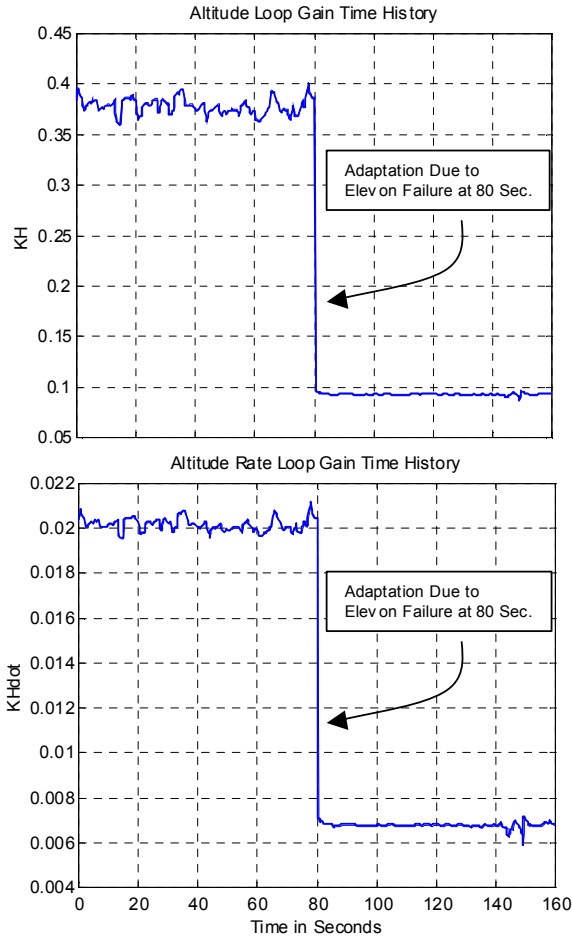


Figure 9. Altitude and Altitude Rate Loop Gain Time Histories.

Figure 10 presents the trajectory for the case of failed elevator with guidance gain adaptation. It can be seen that stability is maintained following the failure at 80 seconds. However, because of the reduced maneuvering capabilities of the vehicle, it can no longer follow the first flare, then overcorrects and lands at a sink rate of  $-20$  ft/sec, (flight path angle of  $-4$  degrees). This would most likely cause severe damage to the vehicle. Methods to remedy this situation are discussed next.

Several preliminary re-targeted trajectories were studied to investigate trajectory/guidance loop interaction. Here, candidate trajectories were designed to abate the required accelerations by increasing the radius of curvature of the first flare. Unfortunately, little improvement was seen in the landing conditions, and only a small reduction in sink rate was achieved.

This study indicates the following:

1. Even if increasing the radius of curvature had been a successful strategy, and such a scheme were to be

implemented, then to cover effector failures throughout the trajectory would require designing re-targeted trajectories at regular intervals throughout the mission segment. Here, the “curse of dimensionality” rules out this approach. It would be a formidable challenge to *manually* design enough re-targeted trajectories such that a viable solution can be found on-line at any time during the mission after an effector failure.

2. The difficulties seen in this case study indicate that the re-targeted trajectory must account for the reduced maneuvering capabilities, be designed to achieve all the final touchdown conditions (ex. sink rate, velocity, etc.), be stored in an efficient manner on-line, and be generated in some automated manner. This leads us to the approach discussed in the next section.

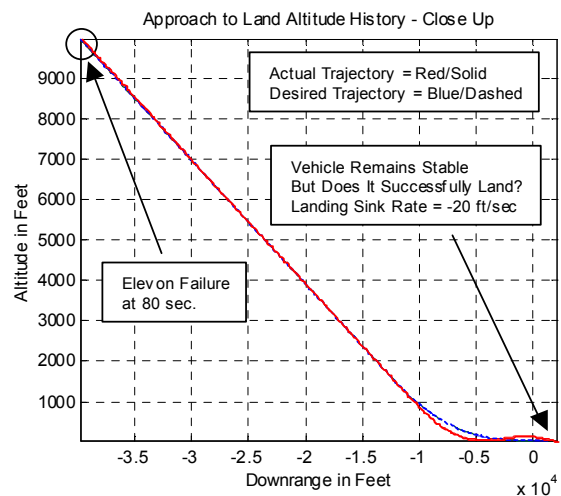


Figure 10. Approach-to-Land Trajectory Under Elevon Failure - With Guidance Reconfiguration.

### Optimum-Path-To-Go/Adaptive Production Guidance (OPTG/APG) Approach

Optimization techniques have been widely studied for *off line* hypersonic vehicle trajectory design [5-11]. Here, on the other hand, the Optimal-Path-To-Go (OPTG) [12-13] algorithm is utilized to generate new reference altitude and altitude rate commands *on-line*. These new commands are designed to be optimal (or near optimal) with the production guidance law structure (feedback loops on altitude and altitude rate), and the adaptive guidance gains (i.e. the APG system discussed previously). Structurally, the feedback loops remain the same as in the APG approach. Now, the

“Reference Command Adaptation Algorithm” block is the OPTG algorithm (see Figure 3).

### OPTG Algorithm Description

The OPTG methodology consists of the following three main elements:

1. Off-Line Trajectory Generation: Form sets of numerous representative optimal trajectories which are valid for the current mission and vehicle capabilities. Here, the Calculus of Variations (COV) [14-15] approach is used to formulate the optimization problem.
2. Off-Line Trajectory Encoding: From the set of neighboring optimal extremals found in Step 1, one has a single set of state-costate pairs that define any given optimal trajectory. Polynomial neural networks can then be employed to learn mappings between the *observable* vehicle states and the costates at different points in the flight space. Not only do the networks provide an efficient, compact “table lookup” that parameterizes the costates as functions of current vehicle *observables* (states and capabilities), but they provide for interpolation between extremals so that on-line, one need not command the vehicle to go to a neighboring extremal, but can instead rapidly generate an approximate extremal trajectory from the current point to the touchdown point.
3. On-Line Trajectory Integration – The final step in the OPTG approach is performed on-line. Trajectories are reshaped in flight to account for changes in the vehicle dynamics. During flight, the current vehicle states are used to compute an appropriate set of costates from the on-board neural network mappings of Step 2. With these states and co-states as starting values, the vehicle dynamics and costate equations are integrated forward for a specified duration and used to compute the new reference trajectories. The loop is closed by re-initializing the costates at regular intervals – typically on the order of 1 Hz. Figure 11 illustrates the parameter space of admissible starting points along the trajectory, and the on-line trajectory reshaping strategy. Note that only two dimensions (altitude and downrange) are illustrated in the figure for clarity. However, for the present formulation, the inputs to the neural networks would include the current altitude, downrange, flight path angle, velocity, identified inner-loop bandwidth and identified drag coefficient. These last two parameters define the current vehicle capabilities and enable on-line trajectory

reconfiguration. From our studies to date, we believe that the outer-loop identification algorithm need only identify a small number of critical parameters, such as inner-closed-loop bandwidth, the total drag on the vehicle, or  $C_{L-max}$ , or the lift-to-drag ratio to convey the vehicle’s “current health” to the PNN model. (It is the job of the inner-loop identification algorithm to identify specific control effector failures and other model details required for *control* reconfiguration.)

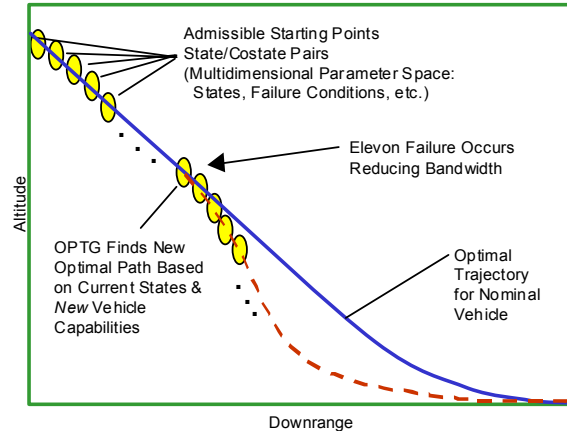


Figure 11. OPTG Trajectory Reshaping Strategy.

This method gives us a solution to the problem found in the case study. Here, entire extremal trajectories can be represented by a single vector of costate variables (or Lagrange multipliers). Then, the pre-trained neural networks can be used to store these costate variables as a function of current vehicle capabilities and states. This provides an efficient way of storing admissible trajectories that start at *any* point in the flight envelope.

### Current Developments

Integration of the OPTG algorithm into the APG system is underway at the time of this writing. Additional model fidelity is also being incorporated. Note in Figure 3 that the velocity dynamics are not included in the block diagram. This simplification implies that a separate velocity control loop is commanding the vehicle’s speed to follow a pre-specified velocity versus downrange profile. The production velocity feedback loop controls speed through PI compensation generating speedbrake commands. However, the failure scenario considered here is a mid-course elevon failure, and an inner-loop control reconfiguration will reallocate pitch control to the only remaining pitch effectors - speedbrake and body flap. Therefore, the speed loop will be affected by an elevon failure.

Figure 12 presents the current formulation for the integrated APG/OPTG guidance system. Here, we no longer model the airframe dynamics with simply one transfer function,  $N_z(s)/N_{zc}(s)$ . Instead, we include the 4<sup>th</sup> order, nonlinear “flight path” guidance equations of motion (also, see Eq. (9) in the next section). Although not indicated, we would also include angle-of-attack dynamics to mimic a stable inner-closed-loop system (analogous to modeling  $N_z$ -to- $N_{zc}$ ).

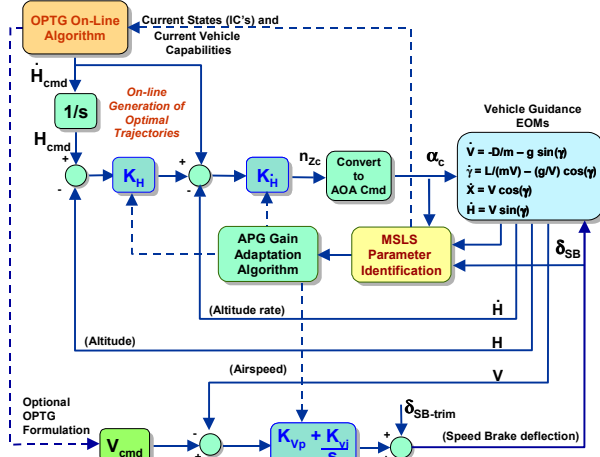


Figure 12. Integrated APG/OPTG Guidance System.

In Figure 12, note that the adaptive altitude production guidance loops remain unchanged. Again, the APG system generates a normal acceleration command. However, since lift and drag,  $L$  and  $D$ , are functions of angle of attack,  $\alpha$ , and elevon, speed brake and body flap deflections,  $\delta_e$ ,  $\delta_{sb}$ ,  $\delta_{bf}$ , it is more natural to drive the guidance dynamics with these variables. Therefore, we convert the normal acceleration command into an equivalent angle-of-attack command. From our aerodynamic model, it can be shown that at each Mach number, there is a linear relationship between  $N_{zc}$  and  $\alpha_c$  (an expected result).

Note the PI compensation in the speed loop and that the speed loop generates a speed-brake deflection command which is fed into the vehicle guidance dynamics. The speed loop itself is driven by a velocity command,  $V_{cmd}$ , which can be derived from an a priori velocity-vs-downrange profile. However, as indicated in the figure, we also allow for an alternate formulation in which the OPTG algorithm generates this command.

The inputs to the MSLS parameter identification algorithm are the states of the system, the angle-of-attack command and the speedbrake command. The outputs of the MSLS algorithm are the critical parameters (such as inner-loop bandwidth) that are used

in the gain adaptation algorithm. Here, the formulation allows for the altitude *and* speed loop gains to be adapted.

Finally, Figure 12 shows that the OPTG algorithm generates a reference or commanded sink rate, and that the reference altitude is obtained by integration. Again, the governing equations for the COV formulation will include the equations of motion, the gain adaptation algorithm, and the altitude and speed loops. One candidate cost function to be minimized is:

$$J = \frac{1}{2} K_1 (\hat{V}_{tf} - V_{tf})^2 + \frac{1}{2} \int_{t_i}^{t_f} \{ K_2 (\dot{H}_{cmd} - \dot{H}_{ref})^2 + K_3 (\dot{H}_{cmd} - \dot{H}_{prev})^2 \} dt \quad (7)$$

Here, the first term in this cost function minimizes the difference between the final velocity and the specified desired value,  $\hat{V}_{tf}$ . The first term in the integrand minimizes the sink rate command from a desired profile,  $\dot{H}_{ref}$ . The second term in the integrand penalizes the difference between the current sink rate command and the previous command value. This term keeps the command rates within reasonable values. If we use the alternate OPTG formulation in which an optimal velocity command is generated, then velocity terms similar to the penalties on sink rate in Eq. (7) would be added to the cost function.

The next step in this work will be to generate numerical results, continuing with the case study discussed herein. Our goal is to generate re-targeted sink rate commands to achieve a softer landing, given that the guidance loops are adapted to address system stability.

A related OPTG approach is presented next.

### Advanced OPTG Approach

For the OPTG/APG formulation, the model of the system consists of the adaptive altitude/rate loops *wrapped around the inner-closed-loop vehicle*. In that formulation, the APG system generates guidance commands into the inner-closed-loop system, and the OPTG algorithm generates trajectory (altitude rate) commands. In contrast, this advanced strategy uses the OPTG algorithm to *directly generate guidance commands into the inner-closed-loop system*. The production guidance loops are discarded. Now, the governing system model for the COV consists only of the inner-closed-loop vehicle (not the production altitude/rate loops). This is considered a more advanced, longer-term approach.

## Case Study: Advanced OPTG Approach

We began our development of the Advanced OPTG approach by generating optimal trajectories for the X-34 during the approach-to-landing phase of flight. The problem was set up such that for the on-line trajectory generation algorithm, an optimal angle of attack command was generated, which was fed directly to the inner-closed-loop system. For this preliminary study, the body flap and speed brake were assumed fixed at their nominal trim values of  $-5^\circ$  and  $60^\circ$ , respectively.

In developing the calculus of variations (COV) to generate optimal trajectories, the case of speed brake failures was investigated. At mid-course in the trajectory, the speed brake was modeled to go from its nominal setting of  $60^\circ$  to its maximum setting of  $90^\circ$ .

The governing equations of motion that were used in the COV derivation are presented next. The conventional “flight path” model governs the velocity and flight path motion, and an approximation to the higher fidelity X-34 aerodynamic force model, provided by Orbital, was used. The states of the system are considered to be:

1.  $V$  = vehicle velocity ~ ft/sec
2.  $\gamma$  = flight path angle ~ radians
3.  $X$  = downrange position ~ feet
4.  $H$  = altitude ~ feet

It can be shown that the governing equations of motion and kinematic relations for this system are:

$$\begin{aligned}\dot{V} &= \left( \frac{-D}{m} - g \sin(\gamma) \right) t_f \\ \dot{\gamma} &= \left( \frac{L}{mV} - \frac{g}{V} \cos(\gamma) \right) t_f \\ \dot{X} &= (V \cos(\gamma)) t_f \\ \dot{H} &= (V \sin(\gamma)) t_f\end{aligned}\quad (9)$$

where,

$$\begin{aligned}L &= \bar{q} S C_L(\alpha, \delta_{sb}, \delta_{bf}), \quad D = \bar{q} S C_D(\alpha, \delta_{sb}, \delta_{bf}) \\ \bar{q} &= 1/2 \rho(H) V^2\end{aligned}\quad (10)$$

Note that the air density model,  $\rho(H)$ , was derived from a Vandenburg AFB atmosphere model supplied by Orbital. Additional governing equations required for the COV formulation are:

$$\begin{aligned}\dot{H}_{lim} &= \left( (H - \hat{H})^2 U(\hat{H} - H) \right) t_f \\ i_f &= 0\end{aligned}\quad (11)$$

Here,  $t_f$  represents a “final time” state and is included in the formulation because this is a free final time problem. This state multiplies the time step and acts to adjust the total integration time. This allows the COV approach to solve for an optimal length of time for completion of the trajectory. In the equation governing the state  $H_{lim}$ ,  $\hat{H}$  is the ground altitude and  $U$  is the unit step function. The function defining  $\dot{H}_{lim}$  can never take on negative values, and takes on positive values if the vehicle ever drops below the ground altitude. The state  $H_{lim}$  was then constrained to be zero at the initial and final times. In order to meet these boundary conditions, this forces the solution to never allow the vehicle to fall below the ground altitude ( $\dot{H}_{lim}$  must remain zero for all time).

Note that lift and drag  $\{L, D\}$  in the above equations are total aerodynamic forces and moments due to non-zero angle of attack and all control surface deflections. To mimic an inner-closed-loop vehicle without specifically accounting for the rotational dynamics in the optimization, the coefficients of lift and drag were approximated by formulas that imply the vehicle is trimmed in pitch. These formulas were derived by curve-fitting data from the high fidelity model of the X-34 aerodynamics, whereby we solved for the trim elevon deflection at each angle-of-attack. Next, we modeled the effect of speed brake deflection (and speed brake failure) as a proportional shift in the value of  $C_D$ . Other nonlinear effects, such as dropping the landing gear, were also included in the drag model. Finally, the angle of attack command was limited to within  $\pm 10^\circ$  to stay within the region where the approximate aerodynamic model is most accurate.

The cost function to be minimized was defined to be:

$$\begin{aligned}J &= \frac{1}{2} K_1 (V_{tf} - \hat{V}_{tf})^2 \\ &+ \frac{1}{2} \int_{t_i}^{t_f} \{ K_2 (\alpha - \alpha_{ref})^2 + K_3 (\alpha - \alpha_{prev})^2 \} dt\end{aligned}\quad (12)$$

This cost function is similar to the one given in Eq. (7). However, now angle-of-attack is the command variable instead of sink rate. Again, the first term in this cost function minimizes the difference between the final velocity and its desired value. The first term in the integrand minimizes the angle of attack control effort from a desired profile  $\alpha_{ref}$  (note,  $\alpha_{ref}$  was derived from nominal trajectories supplied by Orbital), while the second term in the integrand keeps the command rates within reasonable values. Note, the first and second terms in the integrand are not independent, and can be

combined where the objectives are “ranked” by the relative weightings,  $K_2$  and  $K_3$ .

The initial vehicle position is approximately 30,000 ft above the runway, and 20 nautical miles downrange. The final target (runway) altitude is 3,828 feet above sea level. The initial flight path angle is  $-17^\circ$ . We targeted for a final flight path angle of  $0^\circ$  to ensure a minimal sink rate. The initial velocity is 633 fps, and we targeted for a landing velocity of less than 330 fps.

For this proof-of-concept study, two sets of neighboring extremals were generated. One set at the beginning of the trajectory corresponding to the nominal vehicle, and the other set near the point of speed brake failure, corresponding to the vehicle with this failure (increased drag). Figure 13 shows these sets of optimal trajectories. Note that the shooting method [14] was used to obtain optimal trajectory solutions, and relatively little time is needed to generate large sets of neighboring extremals. The engineering challenge comes in finding the *first* valid solution. Two polynomial neural networks were then encoded corresponding to the two sets of trajectories shown in Figure 13, with downrange and altitude as the inputs, and valid co-states as the outputs. For the case study, the first network was interrogated at the beginning of the simulation, and the second was interrogated at the time of failure.

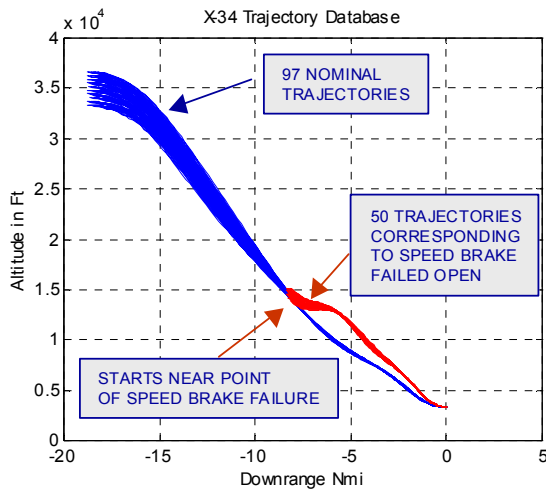


Figure 13. Optimal Trajectory for the Case of Large Drag Deficit.

Figure 14 shows that without reconfiguration, the vehicle is lost, hitting the ground far short of the runway. The added drag due to the speed brake failing wide-open causes a significant reduction in the vehicle’s energy-to-downrange ratio. With the OPTG guidance

system, the vehicle’s flight path is immediately turned up after the speed brake failure to extend the range under the added drag. The final sink rate achieved was less than 7 ft/sec, and the final velocity was actually less than the required final velocity. Note that for the reconfigured trajectory, the vehicle stays aloft approximately 20 seconds longer than for the nominal trajectory. This is due to the increase in angle-of-attack at the point of speedbrake failure, which slows the vehicle down at the same time the sink rate is arrested.

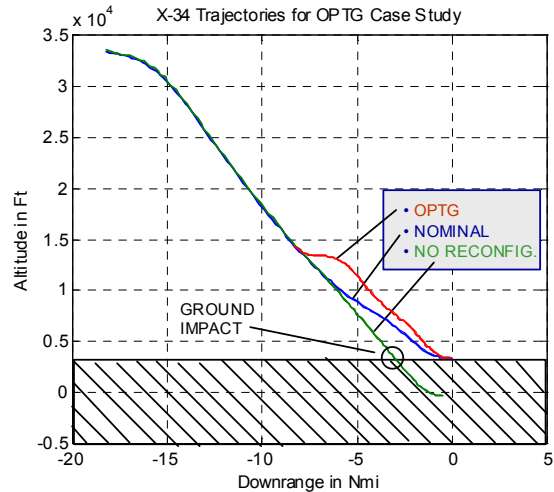


Figure 14. OPTG Trajectory With Speed Brake Failure.

The next step in this formulation is to generate sets of neighboring extremals at regular intervals along the trajectory and encode neural networks corresponding to these sets. The networks should be modeled such that the level of drag is also an input. This would then mechanize the OPTG method to automatically adapt to speed brake failures. Further extensions of the method will include the other states, velocity and flight path angle, and other critical parameters defining the condition of the vehicle (such as inner-closed-loop bandwidth, as discussed previously).

Finally, note that this OPTG approach can be generalized to address not only speed brake failures, but also drag modeling errors and effects of large headwinds or tailwinds. Such effects are of great interest especially at hypersonic conditions where large aerodynamic uncertainties are often encountered.

## Conclusions

Two main formulations of a reconfigurable guidance system for hypersonic RLVs were presented. The Optimal-Path-To-Go/Adaptive Production Guidance (OPTG/APG) system was the first formulation presented. Here, reconfiguration capabilities are

integrated into the current production guidance system to provide flight stability following an effector failure. By utilizing the production guidance system architecture, this approach offers a lower-risk, nearer-term solution to the problem addressed.

A case study developed an APG system for the approach-to-landing problem. Following an elevator failure, the inner-loop reconfigurable control system will reallocate pitch control to the *slower* remaining effectors, thereby reducing the inner-closed-loop bandwidth. The change in this critical parameter was rapidly identified by the Modified Sequential Least Squares (MSLS) algorithm and fed to a guidance gain adaptation law. The gains were properly adapted to maintain stability. However, to achieve a safe landing typically requires re-targeting of the trajectory commands driving the guidance system. We presented a formulation that integrates the APG system with the OPTG algorithm to re-target the altitude rate commands.

The OPTG algorithm employs the calculus of variations to design a large database of admissible neighboring extremals. This database is then efficiently expressed in terms of mappings that generate initial values for the co-states. These mappings are interrogated on-line at regular intervals, updating the optimal trajectory and the corresponding commands required to follow that trajectory.

A more advanced OPTG approach was then presented. Here, the OPTG algorithm was used to generate commands that are fed directly into the closed-inner-loop. A proof-of-concept case study was presented where an optimal angle-of-attack command was generated. The OPTG guidance system was able to land the vehicle safely following a mid-course speed-brake failure that added additional drag to the system.

The case studies indicated promising results for both guidance approaches.

### **Acknowledgements**

This work was funded by an Air Force Phase I SBIR program; Dr. David Doman, AFRL/VACA, Program Manager. *Their support is gratefully appreciated.*

### **References**

[1] Valine, D., "Marshall's X-37 Program Passes First Milestone," *Marshall Star*, Marshall Space Flight Center, March 22, 2001.

[2] Pamadi, B., Brauckmann, G., Ruth, M., "Aerodynamic Characteristics, Database Development and Flight Simulation of the X-34 Vehicle," AIAA Paper No. 2000-0900, *Proceedings, 38<sup>th</sup> Aerospace Sciences Meeting & Exhibit*, Reno, NV, 2000.

[3] Lindberg, R., and R. Feconda, "The X-34: Versatile RLV Technology Test Bed," *Aerospace America*, Aug. 1998.

[4] Ward, D., J. Monaco, and M. Bodson, "Development and flight testing of a parameter identification algorithm for reconfigurable control," *Journal of Guidance, Control, and Dynamics*, Vol. 21, No. 6, Nov. – Dec. 1998, pp. 948-956.

[5] Corban, J., Calise, A., Flandro, G., "Rapid Near-Optimal Aerospace Plane Trajectory Generation and Guidance," *Journal of Guidance, Control, and Dynamics*, Vol. 14, No. 6, 1991, pp. 1181-1190.

[6] Chavez, F., Schmidt, D., "Analytic Aeropropulsive/Aeroelastic Hypersonic-Vehicle Model with Dynamic Analysis," *Journal of Guidance, Control, and Dynamics*, Vol. 17, No. 6, 1994, pp. 1308-1319.

[7] Schmidt, D., "Optimum Mission Performance and Multivariable Flight Guidance for Airbreathing Launch Vehicles," *Journal of Guidance, Control, and Dynamics*, Vol. 20, No. 6, 1997.

[8] Schmidt, D., Lovell, T., "Mission Performance and Design Sensitivities for Hypersonic Airbreathing Vehicles," *Journal of Spacecraft and Rockets*, Vol. 34, No. 2, 1997, pp. 158-164.

[9] Schmidt, D., Hermann, J., "Use of Energy-State Analysis on a Generic Air-Breathing Hypersonic Vehicle," *Journal of Guidance, Control, and Dynamics*, Vol. 21, No. 1, 1998, pp. 71-76.

[10] Lu, P., "Regulation About Time-Varying Trajectories: Precision Entry Guidance Illustrated," *Journal of Guidance, Control, and Dynamics*, Vol. 22, No. 6, 1999, pp. 784-790.

[11] Mease, K., *et. al*, "Re-Entry Trajectory Planning for a Reusable Launch Vehicle," AIAA Paper No. 99-4160, *Proceedings: AIAA Guidance, Navigation, and Control Conf.*, Portland, OR, Aug. 1999.

[12] Ward, D., Monaco, J., Schierman, J., "Reconfigurable control for VTOL UAV shipboard landing," AIAA Paper No. 99-4045, *Proceedings: AIAA Guidance, Navigation, and Control Conf.*, Portland, OR, Aug. 1999.

[13] Bateman, A., D. Ward, R. Barron, J. Monaco, J. Hull, Hydra-7 Guidance Law Development, Barron Associates, Inc. Final Technical Report for Lockheed Martin Advanced Projects, Contract N00174-98-C-0030, Nov. 1999.

[14] Kirk, D., *Optimal Control Theory, An Introduction*, Prentice-Hall Electrical Engineering Series, Englewood Cliffs, New Jersey, 1970.

[15] Pierre, D., *Optimization Theory with Applications*, Dover Publications, Inc., New York, 1986.